JOURNAL OF MATERIALS SCIENCE **35** (2000) 2799–2806

Some peculiarities of fracture of nanocrystalline nitride and boride films

R. A. ANDRIEVSKI, G. V. KALINNIKOV
Institute for New Chemical Problems, Russian Academy of Sciences, Chernogolovka, Moscow Region, 142432, Russia

J. JAUBERTEAU
University of Limoges, Faculty of Sciences, LMCTS-URA 320 CNRS, 123 av. A.Thomas, F-87060 Limoges, France

J. BATES
Institute of Polymer Technology and Materials Engineering, Loughborough University, Loughborough, Leicestershire LE11 3TU, UK
E-mail: ara@icp.ac.ru

Fracture surfaces including those through indentations on different nanocrystalline boride/nitride films were investigated by FE-SEM, conventional SEM, and AFM. TiB_2, TiN, Ti(B,N), AlN, and (Ti,Al)N films have been obtained by non-reactive r.f. magnetron sputtering. Deformation was realized by cleavage fracture and under a Vickers indentor. Two types of film fracture connected with homogeneous and inhomogeneous deformation are described and discussed. The analogy between the inhomogeneous deformation films image and the river pattern in the case of conventional ceramics is also pointed out.

1. Introduction

Unusual properties of nanocrystalline materials (NM) catalyzed the numerous investigations in this field (see, for example, some recent collections and reviews [1–5]). However, the mechanism of NM deformation and fracture is still not clearly understood and needs further consideration. In this connection, fracture surfaces study seems to be useful. Some observations of NM fracture surfaces have been published (e.g. [4, 6–10]). The main results of these observations were: 1) intergranular fracture of NM and 2) the detection of homogeneous and inhomogeneous deformation in the case of cubic (TiN) and hexagonal (TiB_2) films, correspondingly. It is interesting to continue this study and some other subjects using not only Scanning Electron Microscopy (SEM) but Atomic Force Microscopy (AFM) also.

It is worth noting that in recent time the observations of NM inhomogeneous deformation made their appearance (e.g. [11–13]); in so doing localized superplastic deformation of nanocrystalline 3Y-TZP ceramics has been identified by AFM imaging [11]. This technique is now often used to examine surface deformation [14].

2. Experimental details

Films of TiB_2, TiN, Ti(B, N), AlN, and (Ti, Al)N with a thickness of about 1 μm have been prepared on Si substrates using magnetron non-reactive r.f. sputtering. Experimental details, structure and grain size observations have been published elsewhere [15]. Composition and structure of the experimental films are listed in Table I. The approximate chemical formulas of each film were based on the data of the Auger electron spectroscopy (AES) analysis. As evident from the depth profiling analyses with AES, there was satisfactory random distribution of the film components with the exception of only surface layers ($\delta \sim$ 20–30 nm) [16]. It was assumed that all nonmetallic and metallic impurities were substituted separately in the nonmetallic and metallic sublattices correspondingly, and that the films had single-phase composition. The latter was verified by X-ray diffraction and selected-area electron diffraction analyses.

AFM measurements were conducted with a Digital Instruments Nanoscope II operating in constant force mode [17]. A very small tip ($l \sim 2$ nm) attached a cantilever spring ($l = 0.1$) with a froce constant of 0.12 nNm^{-1} touched the surface and the attractive and/or repulsive forces bent the cantilever spring. The deflection of the cantilever was detected by a laser beam. Nanodisplacements were ensured with three piezoelectric ceramics x, y and z which can scaned an area (x, y) of up to 0.13 mm × 0.13 mm. The topography of the sample surface was determined with all the height profiles obtained at each (x, y) scan. The atomic force images of the sample surface were not filtered nor processed; they were just fitted by subtracting a "polynomial plane" consisting of a surface whose cross section was a second order polynomial in one axis and a horizontal line in the other axis. The AFM

TABLE I Composition and structure of films

Sputtering target	Film	Approximate formula	Crystallite size (nm)	Structure type	Parameters (nm)	
					a	*c*
TiB_2	I	$Ti\ (B_{0.92}O_{0.05}C_{0.03})_{1.61}$	5–10	AlB_2	0.3083	0.3246
TiN	II	$(Ti_{0.97}Fe_{0.03})(N_{0.54}O_{0.39}C_{0.11})_{1.48}$	~20	NaCl	0.4292	
$75TiB_2/25TiN$	III	n.d.	n.d.	AlB_2	0.3066	0.3274
A1N	IV	$Al\ (N_{0.78}O_{0.15}C_{0.07})_{0.98}$	n.d.	ZnS_{hex}		n.d.
(Ti, Al)N	V	$(Ti_{0.58}Al_{0.31}Fe_{0.11})(N_{0.73}C_{0.16}O_{0.11})_{1.075}$	n.d.	ZnS_{hex}		n.d.

images of the indentations were not fitted. These indentations were made using a Vickers microhardness tester (Shimadzu type) over the load range (0.5–3) N. Prior to AFM measurements, the indentations were located by means of an optical microscope (×200) and with a lens (×30) fixed on the AFM.

Fracture surfaces of films have been studied also by SEM using both field emission gun high-resolution device (Hitachi S-4000) [7] and a conventional Leica Cambridge Stereoscan S360.

3. Results and discussion

In addition to previous fracture FE SEM images [7, 10], Fig. 1 displays micrographs containing both the formation of shear bands (Fig. 1a and b) and homogeneous

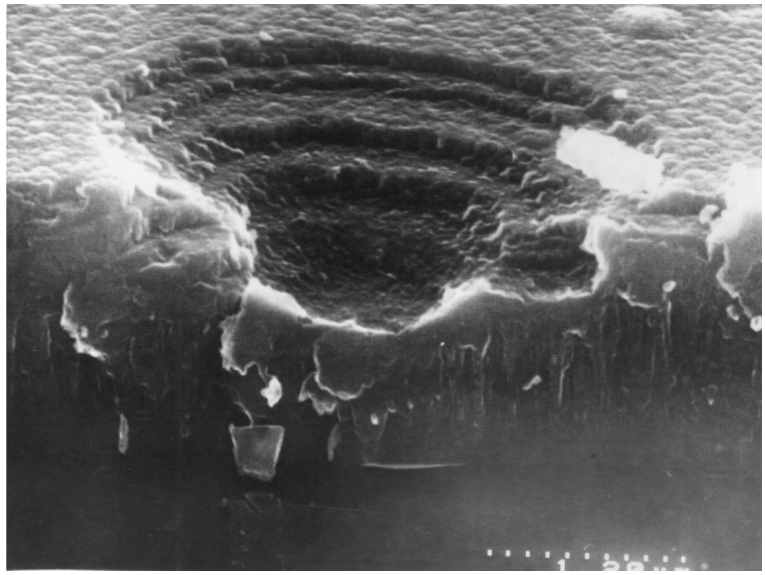

(a)

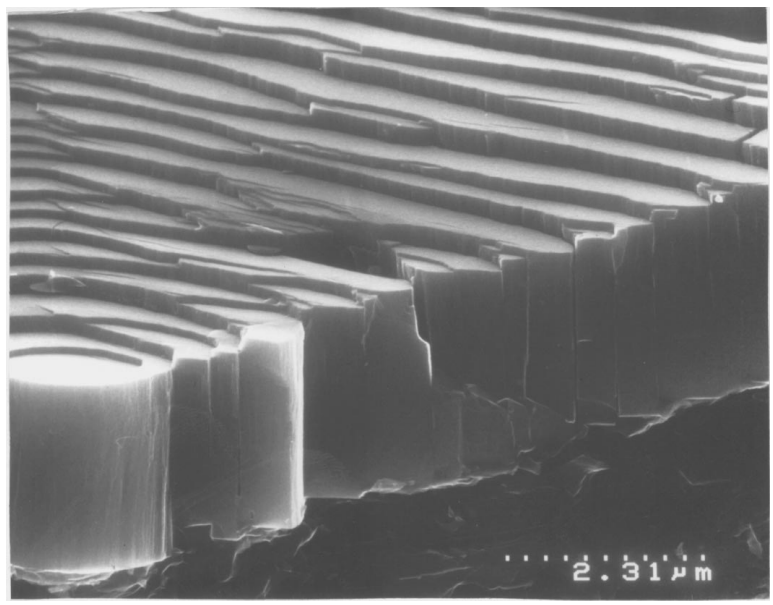

(b)

Figure 1 Fracture FE-SEM images through indentations on (a, b) TiB_2 film I and (c, d) Ti (B,N) film III. Note the formation of steps in the case of TiB_2 film I (a, b). (*Continued*)

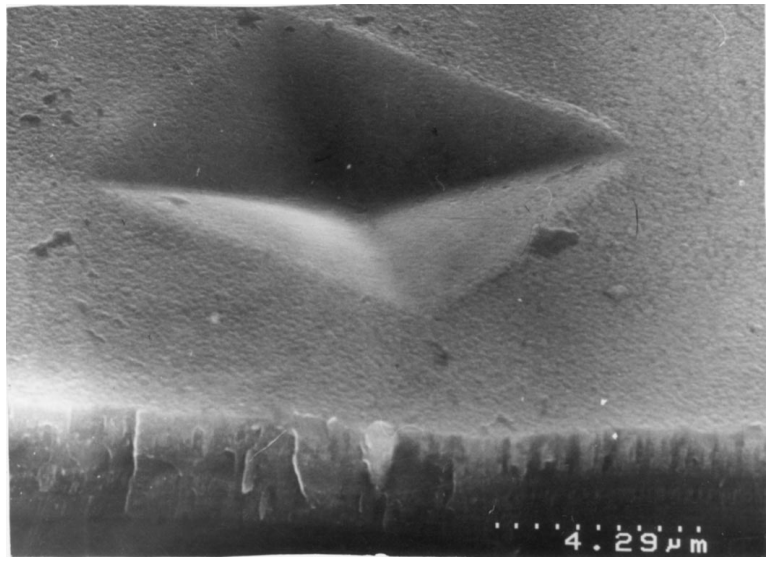

(c)

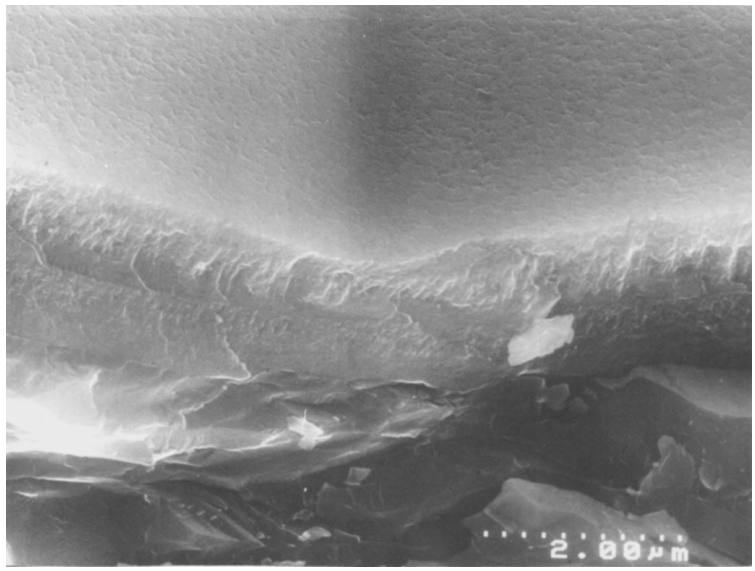

(d)

Figure 1 (*Continued*).

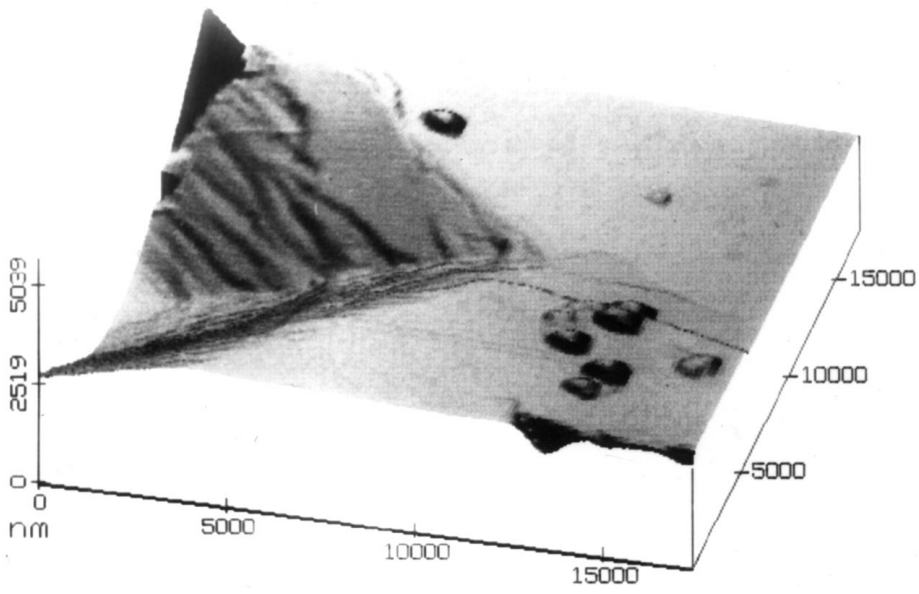

(a)

Figure 2 Three-dimensional AFM images of (a) TiB_2 film I and (b) AlN film IV. (*Continued*)

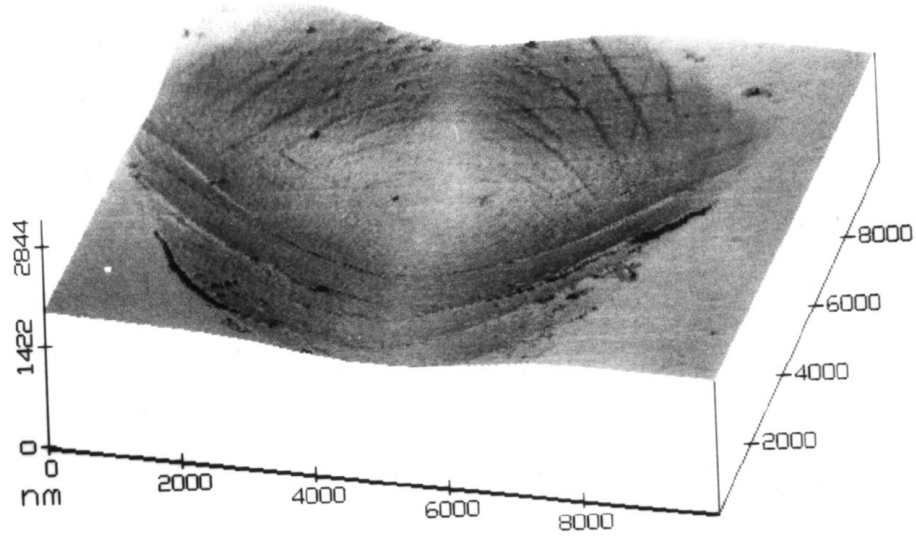

(b)

Figure 2 (*Continued*).

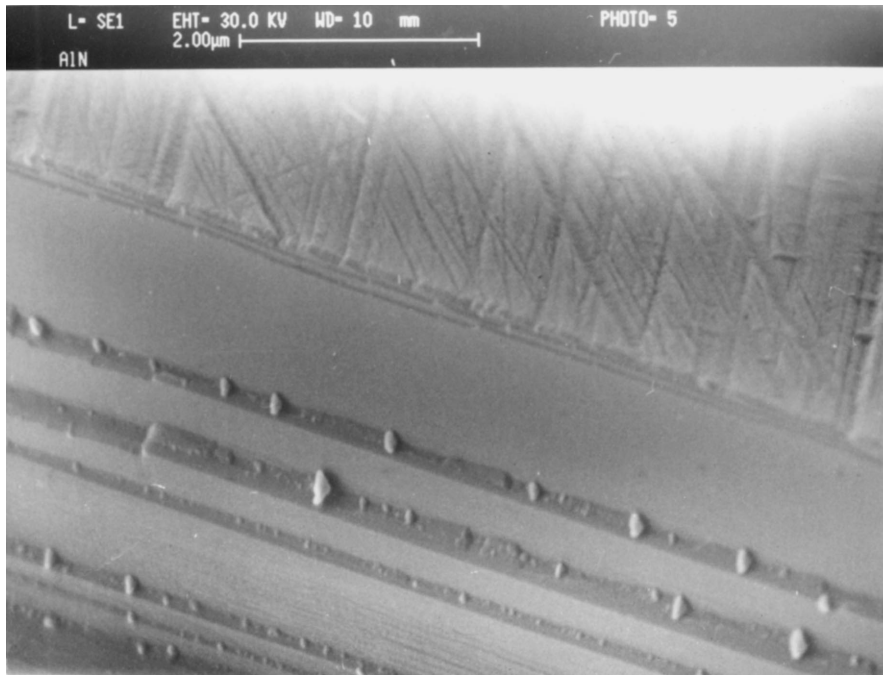

(a)

Figure 3 Fracture SEM images of AlN film IV at different magnifications. There are some breaking-away particles at the steps. (*Continued*)

deformation (Fig. 1c and d) at the indentation and crack surfaces. The difference in deformation was very obvious. However, in contrast to previous results [7, 10], homogeneous deformation was characteristic not only of cubic films but of the hexagonal boron/nitride film III also. Early such deformation was observed only for cubic TiN films [7, 10].

The availability of shear bands on the indentation surface can be observed also by AFM. Fig. 2 shows a step-like surface in the case of TiB_2 film I and the nearly same situation for AlN IV. SEM analysis of the fracture surface of AlN film IV also reveals the step formation as illustrated in Fig. 3.

Using AFM simplifies the estimation of the step sizes. For example, the mean values of the band width and the step height of AlN film IV at the 0.5 N load were about 100 nm and 1000 nm respectively. From previous results [7, 10] and this study, the band width and the step height were changed in a wide interval and ranged from 100 nm to a few hundred nanometers in size.

On the other hand, (Ti, Al)N film V, which also has hexagonal structure as AlN IV is not characterized by step formation and as shown in Fig. 4. The fracture SEM image of (Ti,Al)N film V reveals both inhomogeneous and homogeneous deformation (Fig. 5). It is important to point that the latter is typical for columnar structure. This feature, i.e. homogeneous fracture of TiN type films, has been described in several papers (e.g. [7, 10, 18, 19]). At the same time, inhomogeneous fracture of

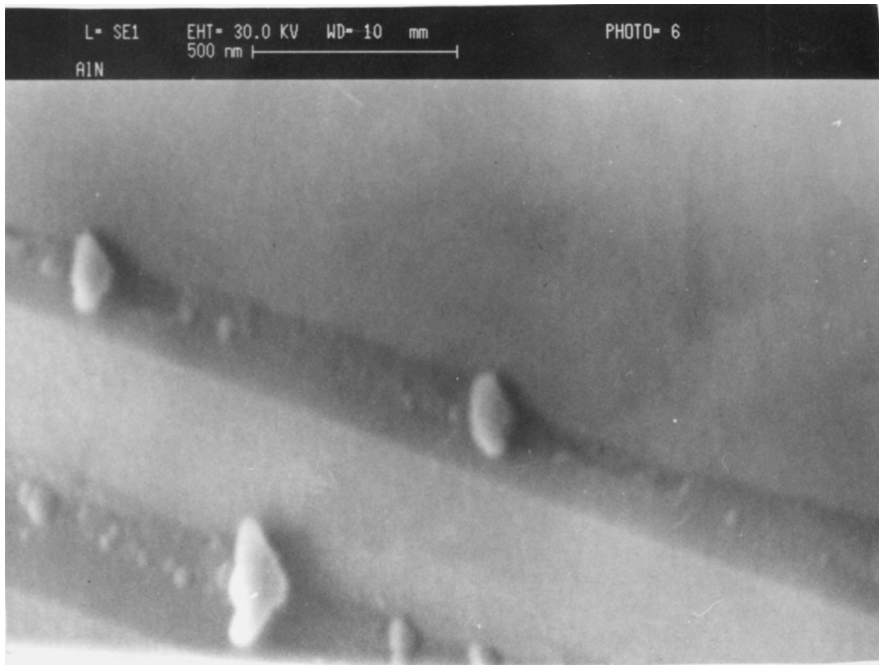

(b)

Figure 3 (*Continued*).

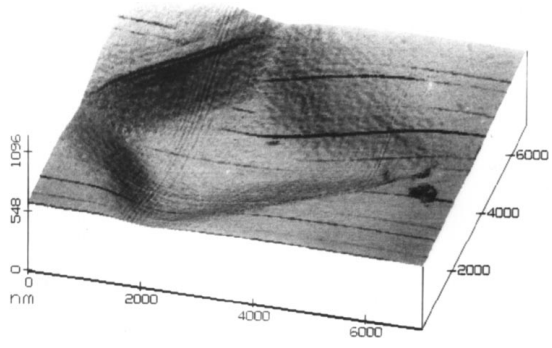

Figure 4 Three-dimensional AFM image of (Ti, Al)N film V.

TiB_2 type films has only been observed in the case of partly columnar or stonelike structure (e.g. [7, 8, 10]). In this sense, (Ti, Al)N film V, as evidenced from Fig. 5, occupies the intermediate place.

In previous discussions of the type of deformation of boride and nitride films, only the difference of the slip systems for TiB_2 and TiN was considered [10]. Notice also that the slip system of TiN is $\{110\}\langle 110\rangle$ rather than $\{111\}\langle 110\rangle$ polyslip (e.g. [20]). Because of the feature of the film compression indentation test, the difference in deformation type for TiB_2 and A1N films, on the one hand, and TiN, Ti(B,N), (Ti, Al)N films, on the other hand, seems to be connected by the presence

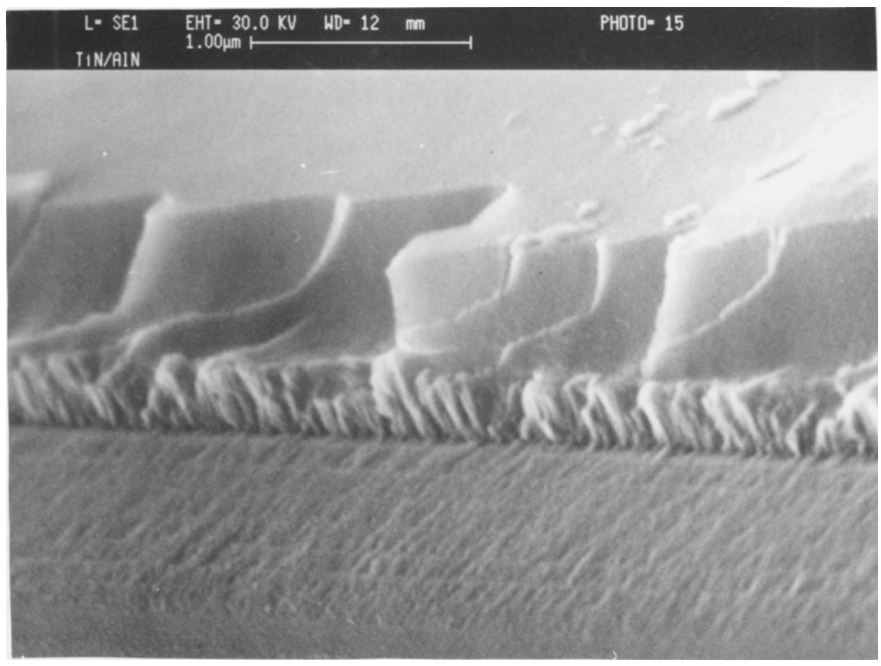

(a)

Figure 5 Fracture SEM images of (Ti, Al)N film V at different magnifications. (*Continued*)

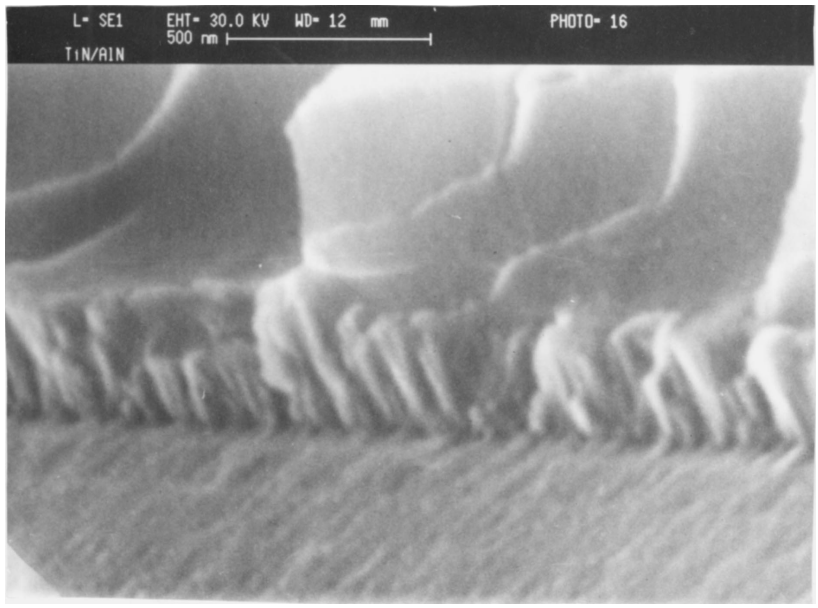

(b)

Figure 5 (*Continued*).

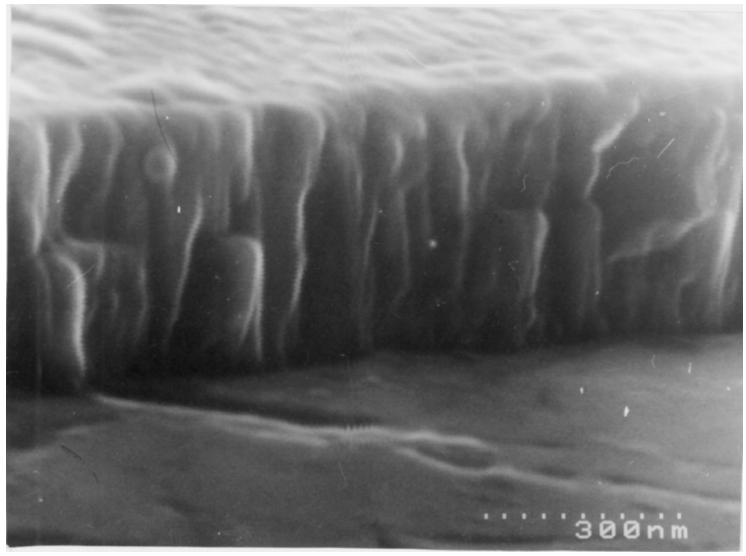

(a)

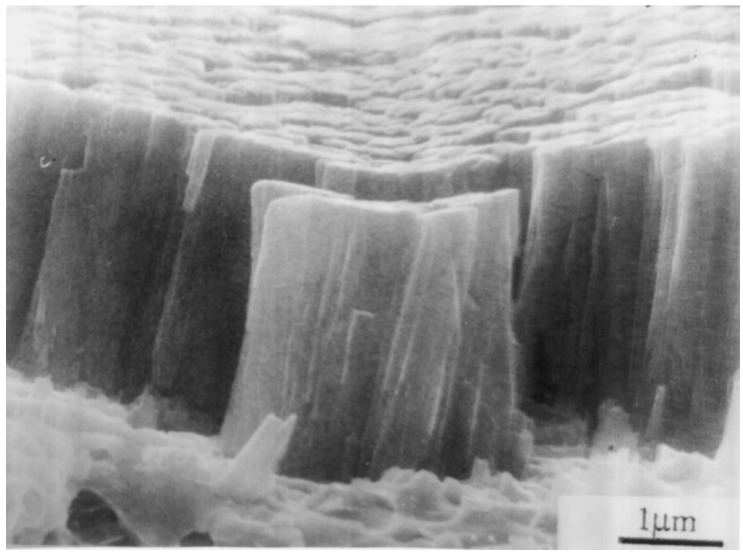

(b)

Figure 6 Fracture SEM images of (a) TiN film II and (b, c) through indentations on TiN [7, 10, 19] films. Note the existence of residual plastic deformation of some TiN columns (c). (*Continued*)

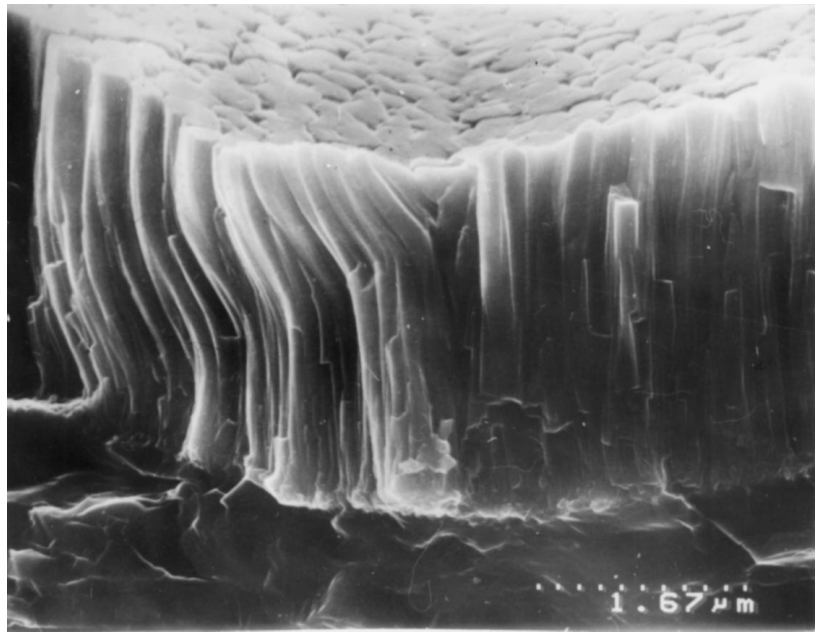

(c)

Figure 6 (*Continued*).

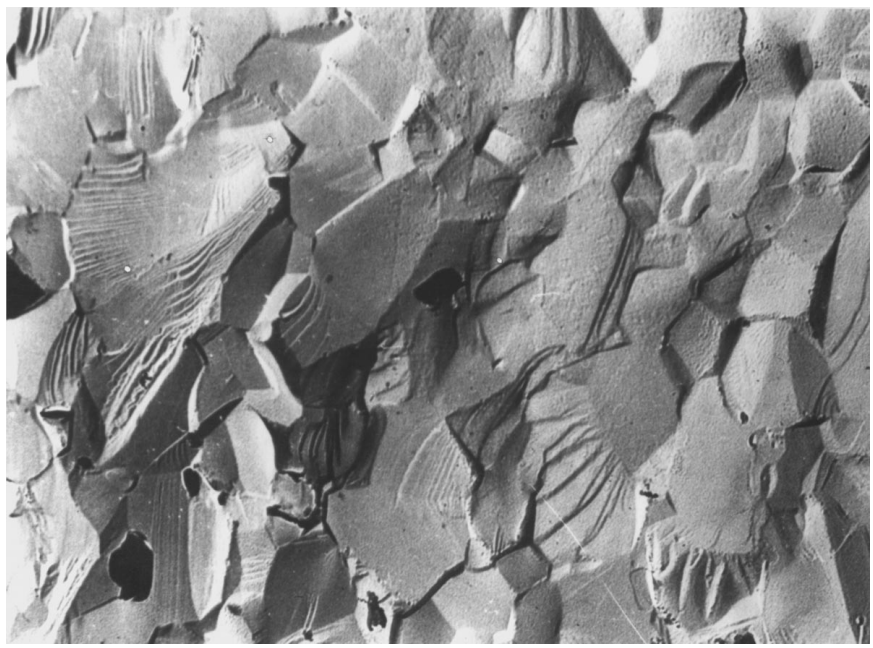

Figure 7 Fracture surface of conventional polycrystalline AlN ceramics (courtesy of Piliankevich *et al.* [22]).

of columnar structures. In the case of clearly defined columnar structure, homogeneous fracture by slip on the boundary columns with the development of brittle (Fig. 6a and b) or residual plastic deformation (Fig. 6c) is dominant and evident.

It should be also recorded that inhomogeneous deformation images, especially Figs 1a, 2a and b, 3a and b, and 5a and b, seem to be similar to those designated as river pattern images. Cleavage steps and the river pattern are well known to be typical for transgranular cleavage fracture when a crack is divided by defects into several separate parts (e.g. [21]). Fig. 7 shows the typical transgranular fracture surface of conventional AlN ceramics [22]. This image was obtained by the two stage replica method. Fracture on well-defined, highly faceted planes of {1120} type is evident and the availability of the step formation and river pattern is also easily observable.

Our statements on the similarity of Figs 1, 2, 3, 5, and 7 as well as on the observation of inhomogeneous deformation for TiB_2 and AlN with partly columnar or stonelike structures do not hold for the nature of inhomogeneous deformation of TiB_2 and AlN films. Intense shear banding observed in these subjects seems to be very similar to behaviour exhibited in other NM (Fe, Fe-Cu, and 3Y-TZP) as well as in amorphous polymers

and metallic glasses [11–13]. Understanding the formation and evolution of the shear bands calls for further investigation.

4. Conclusion

As evident from the foregoing discussion, SEM and AFM studies are effective for investigating the peculiarities of film frature. These methods complement one another. Localized inhomogeneous deformation at the fracture surface and indentation tests with the formation of shear bands has been observed in the case of TiB_2 and AlN films with partly columnar or stonelike structures. Homogeneous deformation at analogous test conditions is typical for films with clearly-defined columnar structures such as TiN, (Ti,Al)N, and (Ti,B)N films. Attention is also called to the similarity of the images of NM inhomogeneous deformation and the river pattern of transgranular cleavage fracture of conventional polycrystalline ceramics.

Acknowledgements

The authors should like to express their thanks to Prof. J. Desmaison (France) as well as Drs. M. Desmaison (France), K. J. Ma (Taiwan), M. Edirisinghe (UK), A. Bloyce (UK), and Mr. D. Hull (UK) for active help in this work. The supports from the INTAS (grant No. 96-2232) and INTEGRATION Program (grant No. 855) are also appreciated.

References

1. A. S. EDELSTEIN and R. C. KAMARATA (eds.), "Nanomaterials: Synthesis, Properties and Applications" (Institute of Physics, Bristol, 1996).
2. G.-M. CHOW and N. I. NOSKOVA (eds.), "Nanostructured Materials: Science & Technology" (Kluwer Academic Publishers, Dordrecht, 1998).
3. A. I. GUSEV, "Nanocrystalline Materials: Preparation Methods and Properties" (Russian Academy of Sciences, Ekaterinburg, 1998) (in Russian).
4. R.A. ANDRIEVSKI, *J. Mater. Sci.* **32** (1997) 4463.
5. E. ARZT, *Acta Mater.* **46** (1998) 5611.
6. Z. LI, S. RAMASAMI, H. HAHN and R. SIEGEL, *Mater. Lett.* **6** (1988) 195.
7. K. J. MA, A. BLOYCE, R. A. ANDRIEVSKI and G. V. KALINNIKOV, *Surf. Coat. Technol.* **94/95** (1997) 322.
8. R. A. ANDRIEVSKI, *J. Solid State Chem.* **133** (1997) 249.
9. *Idem., Nanostruct. Mater.* **9** (1997) 607.
10. *Idem.*, in "Nanostructured Materials: Science & Technology," edited by G.-M. Chow and N. I. Noskova (Kluwer Academic Publishers, Dordrecht, 1998) p. 263.
11. D. S. YAN, Y. S. ZHENG, L. GAO, C. F. ZHU, X. W. WANG, C. L. BAI, L. XU and M. Q. LI, *J. Mater. Sci.* **33** (1998) 2719.
12. J. E. CARSLEY, A. FISHER, W. W. MILLIGAN and E. C. AIFANTIS, *Metall. Mater. Trans. A* **29** (1998) 2261.
13. T. R. MALOW and C. C. KOCH, *ibid.* **29** (1998) 2285.
14. E. FINOT, E. LESNIEWSKA, J.-P. GOUDONNET and J.-C. MUTIN, *Appl. Phys. Lett.* **73** (1998) 2938.
15. R. A. ANDRIEVSKI, G. V. KALINNIKOV, N. P. KOBELEV, JA. M. SOIFER and D. V. SHTANSKY, *Phys. Sol. State* **39** (1997) 1661.
16. R. A. ANDRIEVSKI, in "Surface-Controlled Nanoscale Materials for High-Added-Value Applications," edited by K. E. Gonsalves, M.-I. Baraton, R. Singh, H. Hofmann, J. X. Chen and J. A. Akkara. Vol. 501 (MRS, Warrendale, 1998) p. 149.
17. L. THOMAS, I. JAUBERTEAU, J. L. JAUBERTEAU, M. J. CINELLI, J. AUBRETON and A. CATHERINOT, *Appl. Phys. Lett.* **68** (1996) 1634.
18. M. SHIWA, E. WEPPELMAN, D. MUNZ, M. V. SWAIN and T. KISHI, *J. Mater. Sci.* **31** (1996) 5985.
19. K. J. MA and A. BLOYCE, *Surf. Eng.* **11** (1995) 71.
20. M. ODEN, H. LJUNGCRANTZ and L. HULTMAN, *J. Mater. Res.* **12** (1997) 2134.
21. J. R. LOW, in "Fracture," edited by B. L. Averbach, D. K. Felbeck, G. T. Hahn and D. A. Thomas (MIT and John Wiley & Sons, NY, 1959) p. 68.
22. A. N. PILIANKEVICH, G. S. OLEINIK and V. P. SMIRNOV, *Powder Metallurgy (Kiev)* No. 6 (1981) 69 (in Russian).

Received 19 February
and accepted 28 September 1999